Final Report for Department of Energy Project DE-SC0012198

Period of Performance: 06/01/2014 - 5/31/2017

Probing Electron-Molecule Scattering with HHG: Theory and Experiment

Principal Investigator

Robert R. Lucchese, Department of Chemistry, Texas A&M University, College Station, TX, 77843, lucchese@mail.chem.tamu.edu

Subcontractors

Erwin D. Poliakoff, Department of Chemistry, Louisiana State University, Baton Rouge, LA, 70803, epoliak@lsu.edu

Carlos Trallero-Herrero, J. R. Macdonald Laboratory, Kansas State University, KA 66506, trallero@phys.ksu.edu

Executive Summary

The study of the motion of atoms in molecules is important to understanding many areas of physical and life sciences. Such motion occurs on many different times scales, with electronic motion occurring on a sub-femtosecond time scale, and simple vibrational motion in tens to hundreds of femtoseconds. One way to follow such processes in real time is by the use of short-pulsed lasers, and in particular by studying time-resolved photoionization and the related process of high-harmonic generation (HHG). Thus there has been much effort to develop the tools necessary to probe molecular systems using short pulse lasers and understanding the sensitivity of the different possible probes to the time dependent geometric structure as well as the electronic structure of molecules. Our research has particularly focused on the connection between high-field processes and the more traditional weak field photoionization processes. Strong field and weak field processes can be connected through models that involve the same matrix elements. We have demonstrated in our study of HHG from SF_6 that the spectrum is sensitive to the interplay between the angular dependence of the ionization step and recombination step. In our study of rescattering spectroscopy, we have shown that with a combination of experiment and theory, we can use this high-field spectroscopy to determine molecular structure in molecules such as C_2H_4. We have also developed new computational tools based on overset grids to enable studies on larger molecular systems which use much more robust numerical approaches so that the resulting code can be a tool that non-specialists can use to study related systems.

Comparison of Actual Accomplishments with Proposed Goals and Objectives

In the original proposal there were three main goals. The first goal was experimental studies of high harmonic generation (HHG). In this area, there was less progress than was anticipated. We note that the subcontract for the experimental work changed when Erwin

Poliakoff withdrew from the project after the first year and Carlos Trallero-Herrero became a subcontractor in the third year. We did complete and publish the experimental HHG work that was ongoing at the beginning of the project, but later when the Trallero-Herrero became the subcontractor, the experimental emphasis became the comparison high-field and weak-field ionization as well as instrumental development.

The second goal was to make a detailed comparison between different levels of theory for the HHG yield and experimental data for molecular systems to understand which processes in molecular photo-recombination have an effect on the observed HHG yield. In this area we have published a detailed comparison of experimental HHG spectra of SF_6 and computed recombination rates. We found that the combination of the molecular frame strong-field ionization rates as a function of field and electron emission direction and the molecular frame recombination rates also as a function of angle of incidence of the recombining electron controlled the HHG yield. We also published a study that made a connection between the ellipticity of the exciting light and HHG produced which could be related to the photoelectron asymmetry parameter for the photoionization of Ar.

The third goal was to develop a new grid based complex Kohn computer code to allow for converged results for electron-molecule collisions on larger systems when compared to the methods currently used. Towards this goal we have made significant progress. This work was performed in close collaboration with Atomic, Molecular, and Optical (AMO) theory group at Lawrence Berkeley National Laboratory (LBNL). Although the numerical methods that we finally developed are somewhat different from what was originally proposed, we have found an approach that has already allowed us to successfully implement a grid based complex Kohn method for static-exchange level calculations.

In addition to these specific goals, we also indicated that we would pursue a number of other theoretical studies involving high-field and weak-field ionization processes. In particular in the area of high-field processes, we have completed studies on rescattering spectroscopy for structural determination and a study of the coherence of electronic states of a molecule produced by very short excitation pulses. Finally we have also completed a series of more traditional experimental and theoretical studies on weak-field photoionization.

Project Activities

In the description of the project activities, citations in square brackets [] refer to the publications listed in the Products Developed section that contain the full details of the work summarized here.

Atomic HHG

With respect to high harmonic spectra, we have worked on both atomic and molecular targets. In particular, we have worked with Tony Starace at the University of Nebraska and his collaborators in order to develop methods for extracting photoionization data quantitatively from HHG spectra via ellipticity measurements [6]. More specifically, we have shown that it is possible to extract photoionization asymmetry parameters via measurements of the ellipticity dependence of HHG spectra. An example of the data that are acquired for such a procedure is shown below in Fig. 1 for the case of HHG in atomic Ar. Here we show the intensity of the HHG yield as a function of the degree of ellipticity of the exciting laser. Normally, the exciting lasers in HHG generation have linearly polarized light. This high-field process can be modeled using the usual three step model of the HHG process, i.e. tunnel ionization, propagation of the

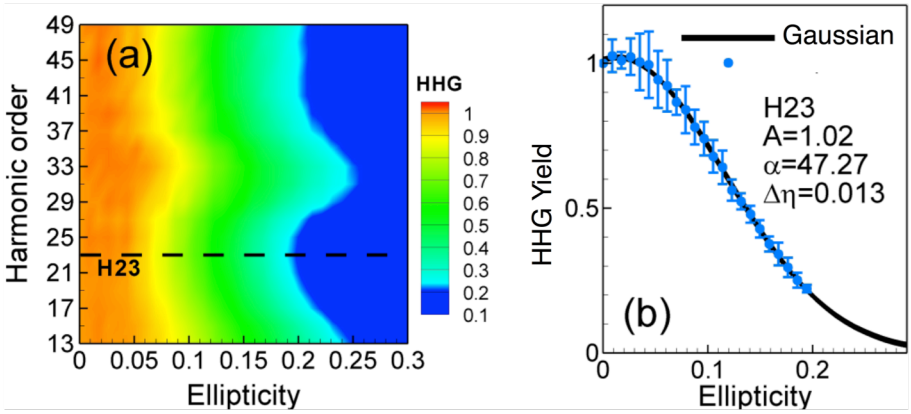

Figure 1. Normalized HHG yield for Ar vs. ellipticity for λ=0.78 μm at an intensity of 3.8×10^{14} W/cm^2.

electron away form the atom or molecule and then back towards the molecule under the influencing of the oscillating laser field, then photo-recombination in the case of HHG or scattering in the case of rescattering spectroscopy. In this picture, if the exciting laser field is not linearly polarized, the electron being driven back towards its source will acquire transverse momentum and then not return to the vicinity of the source atom or molecule. However if the ellipticity is not too large, the dependence of the yield, $\hat{Y}$, on the ellipticity can be modeled as a Gaussian of the form

$$\hat{Y}(\eta) = Ae^{-\alpha(\eta-\Delta\eta)^2}, \qquad (1)$$

where η is the ellipticity and $\Delta\eta$ is a fitting parameter which accounts for the small uncertainty in the experimental determination of the ellipticity. The fit to the ellipticity data using Eq. (1) is shown on the right-hand panel of Fig. 1.

Using the theoretical framework developed by the University of Nebraska collaboration, it was possible to extract photoelectron asymmetry parameters from data such as those shown in Fig. 1, and the results from such a procedure are shown for the Ar example in Fig. 2. The comparison with previously obtained photoionization data is very good.

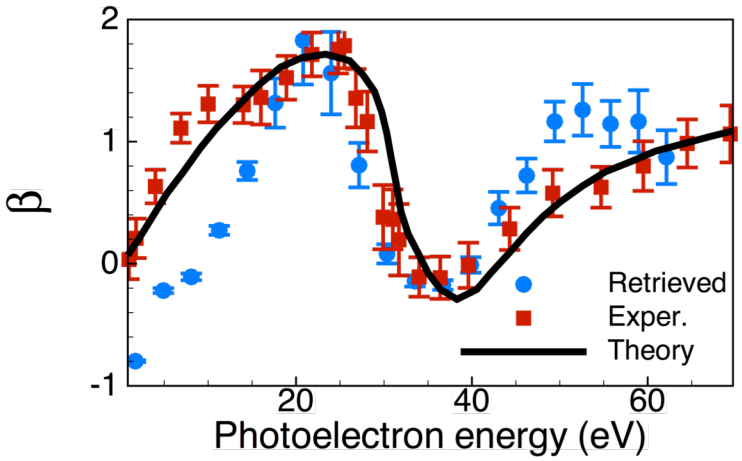

Figure 2. Energy dependence of the Ar 3p subshell photoelectron asymmetry parameter $\beta(E)$. Solid line: RPAE theoretical results[1]; red squares: experimental photoionization results[2]; blue circles: present results retrieved from HHG spectra.

Molecular Aspects of HHG

We have studied HHG in relatively complex molecules, in particular we have completed a study of HHG in SF_6 [8]. Experimentally we have considered a wide variation of both the intensity of the exciting laser and the position of its focus relative to the gas jet. The main qualitatively feature seen in the measured HHG yield, shown in Fig. 3, is a narrow peak centered at 23 eV (H15) and a broad peak centered at 32 eV (H21). These two features were observed under almost all of the conditions considered.

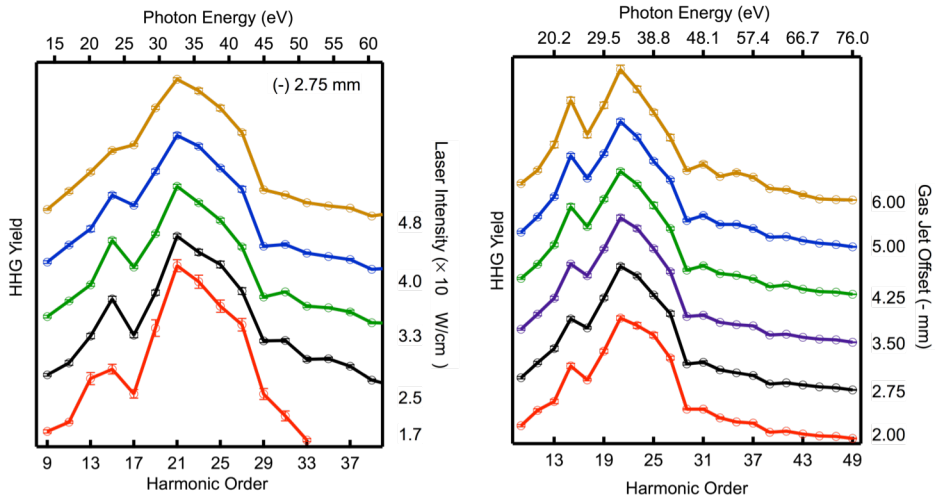

Figure 3. Sensitivity of experimental HHG signal in SF_6 with respect to the intensity of the exciting laser and positioning of the focus of the laser with respect to the medium.

Theoretically we have applied the quantitative rescattering (QRS) theory[3,4] to isolated SF_6 molecules and considered the excitation of the electrons from the three most weakly bound orbitals, i.e. the highest occupied molecule orbital $1t_{1g}$ (HOMO), $5t_{1u}$ (HOMO-1), and $1t_{2u}$ (HOMO-2) orbitals. These three orbitals have ionization potentials that are all within 1.5 eV of each other. For the recombination step in the three-step model, which is the basis of the QRS, we have considered results from relatively simple single-channel static-exchange type calculations and from coupled-channel calculations that include dynamic electron correlation effects. In the HHG process for molecular targets, each molecule in the excited medium can emit light with a different phase depending on the orientation of the molecule in the exciting medium relative to the polarization direction of the exciting laser. The HHG signal is then obtained by a coherent average over all possible orientation of the molecules. The full expression of the HHG power spectrum within the QRS model is then

$$S(\omega)=\frac{2\omega^4}{3\pi c^3}\left|\sum_i g_i X_i^{\mathrm{ref}}(\omega)\frac{1}{4\pi}\int_0^{\pi}d\theta\int_0^{2\pi}d\phi\,\sin\theta\left[N_i(\theta,\phi)\right]^{\frac{1}{2}}e^{i\Delta\eta_i(E_i,\theta,\phi)}d_i(\omega,\theta,\phi)\right|^2 \qquad (2)$$

where $X_i^{\mathrm{ref}}(\omega)$ is the amplitude of the returning wave packet at frequency ω from a reference atom subjected to the same field, g_i is the degeneracy of the active orbital labeled by the index i, $N_i(\theta,\phi)$ is the tunneling rate in the direction (θ,ϕ), $d_i(\omega,\theta,\phi)$ is the photo-recombination transition dipole, and $\Delta\eta$ is the phase of the tunneling electron. To investigate the coherence of the different parts of the expression given in Eq. (2), we have considered two simpler expression

for the power spectrum. First we considered an incoherent sum over the different ionization channels of the form

$$S'(\omega) = \frac{2\omega^4}{3\pi c^3} \sum_i g_i^2 \left| X_i^{\text{ref}}(\omega) \right|^2 \left| \frac{1}{4\pi} \int_0^{\pi} d\theta \int_0^{2\pi} d\phi \sin\theta \left[N_i(\theta,\phi) \right]^{\frac{1}{2}} e^{i\Delta\eta_i(E_i,\theta,\phi)} d_i(\omega,\theta,\phi) \right|^2 . \quad (3)$$

Alternatively, if only the total cross section and total tunneling rates are know, or can be estimated, then the following expression, which is a completely incoherent product of the amplitudes of the steps in the QRS model, is commonly used

$$S''(\omega) = \sum_i \frac{2\omega^4 \left| X_i^{\text{ref}}(\omega) \right|^2}{3\pi c^3} \bar{N}_i \frac{\sigma_i(\omega)}{4\pi} \frac{c}{4\pi^2 \omega} . \quad (4)$$

where $\bar{N}_i$ is the average tunneling rate from active orbital *i*, σ_i is the total photoionization cross section from orbital *i*.

The QRS results with orientation averaging included in Eq. (3) and (4) are shown in Fig. 4. Additionally in Fig. 4 we show results for both frozen-core Hartree-Fock (FCHF) calculations, in which all ionization channels are treated separately, and multi-channel FCHF (MCFCHF) calculations, which include some electron correlation effects. Finally we also show the corresponding total cross sections to indicate the relationship between the photoionization cross section and the HHG yield. In the middle column of Fig. 4 we show the results for a

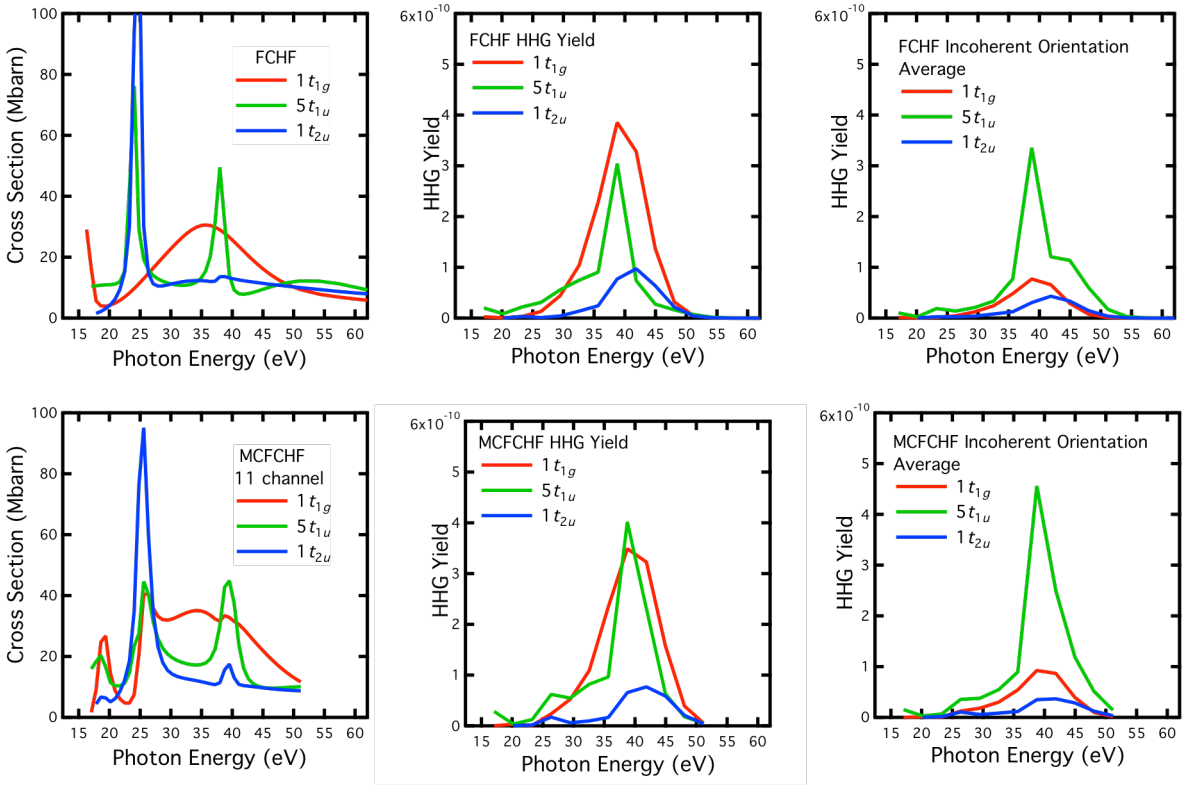

Figure 4. Photoionization cross sections and QRS HHG spectra of SF_6 for the outer three valence orbitals, $1t_{1g}$ (HOMO), $5t_{1u}$ (HOMO-1), and $1t_{2u}$ (HOMO-2). Left column is the computed photoionization cross sections. Center column is the QRS HHG spectra from the different channel terms in Eq. (3), which has a coherent orientation average. Right column is the approximate separate-channel HHG spectra obtained from the incoherent orientation average given in Eq. (4). The top row contains the results for the single-channel FCHF calculations and the bottom row has the corresponding data from the coupled channel MCFCHF calculations.

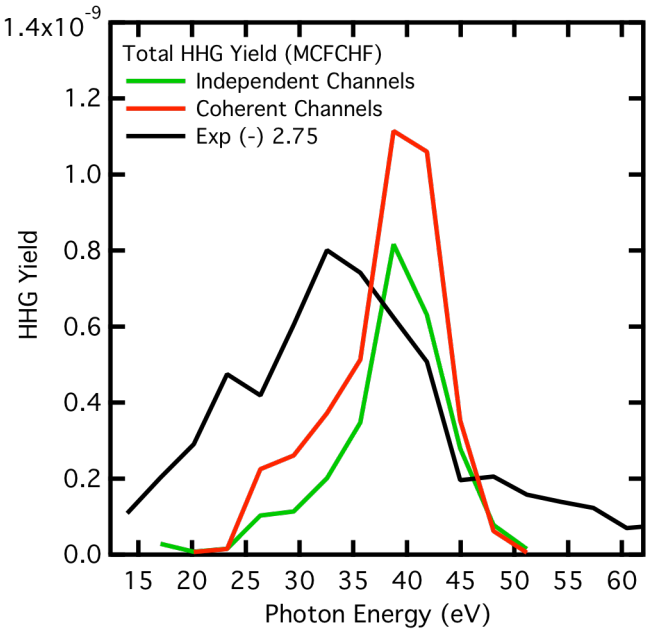

Figure 5. Comparison of HHG yield computed from the incoherent sum from the different channels using Eq. (3) (green), the coherent sum over the channels with the appropriate phases using Eq. (2) (red), and the experimental results (black) with laser intensity of 4.0×10^{14} W/cm^2 with the focal point at (-)2.75 mm.

coherent orientation average but where the different channels are treated separately, this is equivalent to plotting the separate-channel contributions to S' as defined in Eq. (3). The calculated HHG yields from the $1t_{1g}$ and $5t_{1u}$ subshells, in both the FCHF and MCFCHF calculations, exhibit a peak centered near 40 eV (H25). The HHG from the $1t_{1g}$ (HOMO) is strong in this energy region due to the broad kt_{2u} shape resonance present in the $1t_{1g}$ photoionization cross section, as shown in the left column of the figure, whereas the $5t_{1u}$ (HOMO-1) is enhanced by a narrow shape resonance in the ke_g continuum. The computed QRS spectra are on the same scale and are plotted as the power spectrum in atomic units. Thus, while it is clear that contributions from the $1t_{1g}$ (HOMO) and $5t_{1u}$ (HOMO-1) both make substantial contributions to the harmonic yield at most harmonic orders, the shape resonance from the $5t_{1u}$ and $1t_{2u}$ orbitals at 26 eV (H17) enhances the harmonic yield near these resonances.

We have also computed the separate-channel HHG spectra using the incoherent orientation averages, S'', as given in Eq. (4), and as shown in the two panels in the right column of Fig. 4. Comparing these results to the QRS HHG in the middle panels, obtained with the correct orientation average, we see that the incoherent orientation average has many of the same features. However the two calculations have dramatically different relative intensities, in particular the $1t_{1g}$ (HOMO) and $5t_{1u}$ (HOMO-1) channels have very similar peak intensities using the coherent orientation average, whereas in the QRS calculation with the incoherent orientation average the $5t_{1u}$ (HOMO-1) peak is about five times stronger than the peak $1t_{1g}$ (HOMO).

Finally, in Fig. 5, we present the coherent channel sum as given in Eq. (2) for the MCFCHF QRS calculation. We can see that the coherent channel sum leads to an enhancement in the HHG signal with only minor changes in the qualitative features of the spectrum.

Overall we can qualitatively understand the peaks seen in the experiment at 23 eV and 33 eV. However in the computed results, the resonance features are shifted to higher energy compared to the experiment, and the low-energy feature at ~23 eV, is somewhat more pronounced than in our best calculation, which is the MCFCHF with a coherent sum of the amplitudes for the three channels.

Grid Based Electron-Molecule Scattering Calculations

An important component of our research program is the development of a next-generation electron-molecule scattering code [13]. This work is being done in collaboration with the AMO theory group at LBNL, led by Bill McCurdy. This code is based on the complex Kohn approach with a numerical grid-based representation of the scattering wave functions. We employ an overset grid representation where there is one central spherical grid and centered on each nucleus in a molecule there is an additional local grid that has spherical symmetry around that center, as illustrated in Fig. 6. We have successfully implemented the overset grid method at the static-exchange calculation level.

The Kohn stationary functional, $T^{+S}_{\mathbf{k}',\mathbf{k}}$, of the trial functions, $\psi^{(+)t}_{\mathbf{k}}$ and $\psi^{(-)t}_{\mathbf{k}'}$, is

$$T^{+S}_{\mathbf{k}',\mathbf{k}} = T^{+t}_{\mathbf{k}',\mathbf{k}} + (2\pi)^{-\frac{3}{2}} \left\langle \psi^{(-)t}_{\mathbf{k}'} \middle| \hat{H} - E \middle| \psi^{(+)t}_{\mathbf{k}} \right\rangle \tag{5}$$

where $T^{+t}_{\mathbf{k}',\mathbf{k}}$ gives the asymptotic form of $\psi^{(+)t}_{\mathbf{k}}$. Then expanding the trial functions in linear combinations of basis functions and requiring $T^{+S}_{\mathbf{k}',\mathbf{k}}$ to be stationary with respect to variations in the linear expansion coefficients leads to an expression for $\mathbf{T}^{S}$, using a matrix notation, of the form

$$\mathbf{T}^{S} = \mathbf{N}_{00} - \mathbf{N}_{0q}\mathbf{M}^{-1}_{qq}\mathbf{N}_{q0}, \tag{6}$$

where the subscript 0 denotes the set of regular unscattered continuum functions, the subscript q denotes the expansion basis set, which contains asymptotic scattered wave boundary conditions, **N** denotes matrix elements of the interaction potential, and **M** contains matrix elements of $\left(\hat{H} - E\right)$.

In earlier implementations of the complex Kohn method,[5,6] the trial functions were constructed from a linear combination of atomic-centered Gaussian type functions with additional long-ranged functions constructed to represent the scattered wave. Although this approach was very efficient and could use much of the computational machinery that has been developed for traditional bound state quantum chemistry methods, there are two significant limitations. First, the non-local exchange interaction was approximated using a separable approximation. This in general works well, however it is liable to uncontrolled errors at low scattering energies, below about 1 eV. The second limitation of the Gaussian basis set approach is the difficulty in applying the method to high kinetic energy electrons, above ~50 eV, since it is difficult to construct functions which have high partial waves and significant radial oscillations using just atomic centered Gaussians, as is required to represent such higher kinetic energy electrons. One solution to the limitations is to represent the scattering functions on numerical grids. Such grids can be easily made dense enough in both the angular and radial directions to converge the calculations at low and high energy.

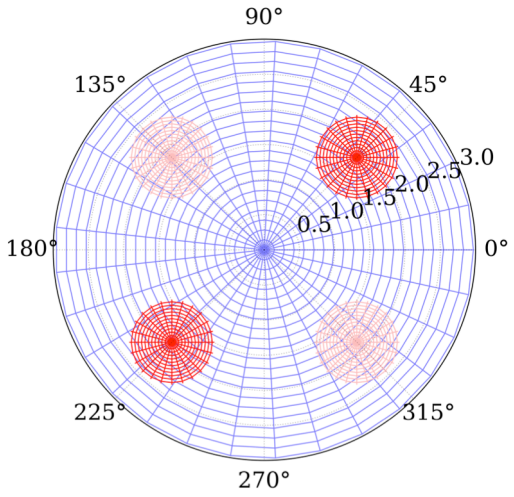

Figure 6. Sketch of the overset grid for CF_4. The red spheres are centered on the F atoms and the larger central grid is centered on the C atom.

The grids we use are combinations of finite-element-method discrete-variable-representation (FEM-DVR) grids for the radial variable in each subgrid with Gauss-Chebyshev and Gauss-Legendre quadratures in the angular variables. A wave function described everywhere in space can be switched onto the each grid g using Becke switching functions, W_g, commonly used in numerical density functional calculations, that smoothly switch between unity inside the grid and zero outside it,

$$\Psi(\mathbf{r}) = \sum_g W_g(\mathbf{r})\Psi(\mathbf{r}) . \tag{7}$$

The left-hand and right-hand sides of Eq. (7) are equal because the switching functions sum to unity everywhere in space,

$$\sum_g W_g(\mathbf{r}) = 1 . \tag{8}$$

The right-hand side of Eq. (7) is a sum of wave functions localized on each grid,

$$\psi_g(\mathbf{r} - \mathbf{r}_{g,0}) = W_g(\mathbf{r})\Psi(\mathbf{r}) , \tag{9}$$

where $\mathbf{r}_{g,0}$ is the origin of grid g. The localized functions can then be expanded in local partial waves. Now each operator needed to evaluate the complex Kohn variation expression can be evaluated by sums of terms where for each term the operator is expressed about a different center using the expansion about that center. This approach is much more rapidly convergent than a single-center expansion about a single center, as was used in our earlier Schwinger electron-molecule scattering codes.[7]

Combined with the grids and the complex Kohn variational method, we also require a basis set. One could just use the polynomial basis sets in radial direction that naturally accompany the FEM-DVR radial grids combined with the spherical harmonics that are the appropriate spectral functions to accompany the Gauss-Chebyshev and Gauss-Legendre angular

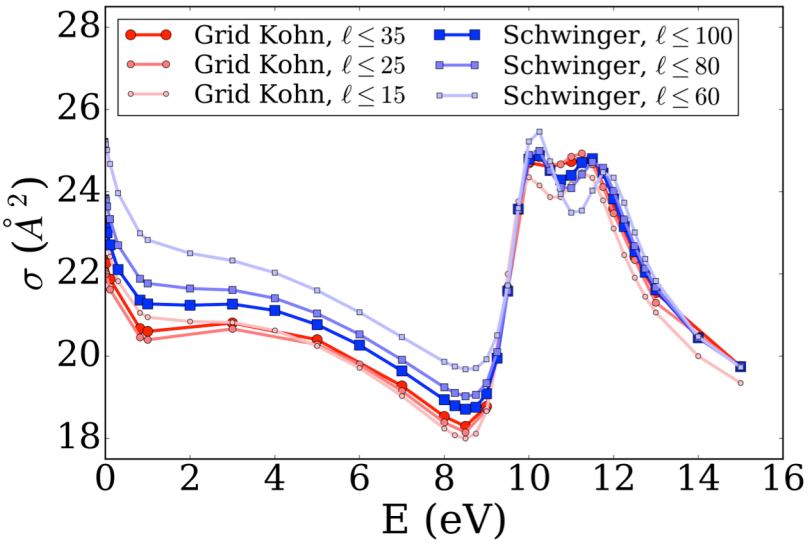

Figure 7. Comparison of the cross sections for the static-exchange potential of CF_4. The grid Kohn method (red circles, various fading) are given for subgrids with l=3 and central grid with l = 15, 25, and 35. The non-resonance features match for all three, while the resonance features converge at l = 25. The single-center expanded Schwinger method (blue squares, various fading) is shown for l = 60, 80, and 100 for which some of the features are not converged even for maximum l = 100.

grids. Doing this leads to linear equations of the type given in Eq. (6) that can be on the order of millions by millions. Inverting these equations can be quite computationally intensive. We have found an alternative approach where we construct a basis set for the scattering problem directly on the grid. In particular, in a partial-wave representation, the trial function $\left|\psi_{klm}^{(\pm)t}\right\rangle$ is written as

$$\left|\psi_{klm}^{(\pm)t}\right\rangle = \left|\phi_{klm}^{0}\right\rangle + \sum_{i=1}^{N} c_i \left|\phi_{i,klm}^{(\pm)}\right\rangle$$
$$\left|\phi_{i,klm}^{(\pm)}\right\rangle \equiv (\hat{G}_0^{\pm}\hat{V})^i \left|\phi_{klm}^{0}\right\rangle \tag{10}$$

where the c_i are the linear variational parameters, $\hat{G}_0^+$ is the free-particle Green's function, $\hat{V}$ is the interaction potential, and $\left|\phi_{klm}^{0}\right\rangle$ are the un-scattered continuum functions, i.e. spherical Bessel functions. Using this basis set leads to very rapid convergence with respect to increasing N, typically only requiring 15 to 20 functions. We have shown that this rapid convergence is due to the fact that this basis set leads to $\left[(N-1)/N\right]$ Padé approximant to the scattering T-matrix.

We have tested the grid complex Kohn approach on electron-scattering from CH_4 and CF_4. In Fig. 7 for e-CF_4 scattering, we see that the grid Kohn converges to essentially to the correct answer with only partial waves up to $l = 25$ in the central grid compared to the Schwinger results with a single-center expansion which was not converged with a partial wave expansion including up to $l = 100$.

Field ionization of molecular isomers: weak vs strong field

Strong-field ionization of atoms and molecules occurs when one or more electrons are stripped from the parent molecule by an electric field of a relatively low frequency.[8] Unlike photoionization by single photons where the field can be very weak, in the strong-field limit, the

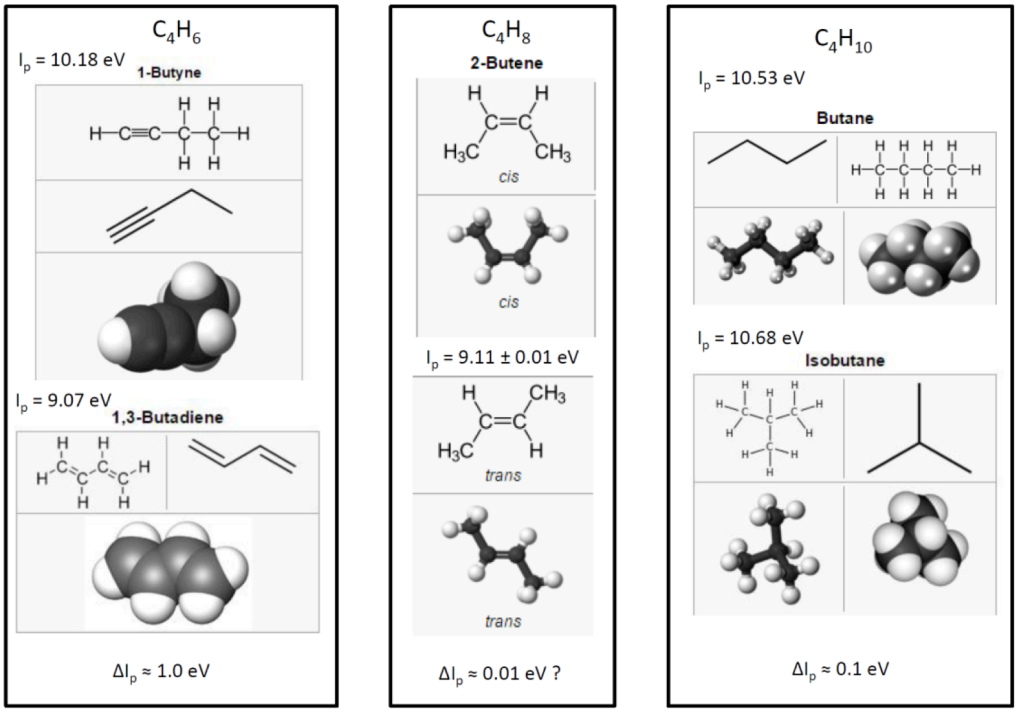

Figure 8. The three pairs of molecular isomers studied with the corresponding ionization potentials I_p and the difference in ionization potential ΔI_p.

binding potential of the electron is distorted by the field. This difference poses the question of the sensitivity of strong-field ionization to the molecular structure. While the sensitivity of strong-field ionization to molecular orbitals has been demonstrated [9-11], the limits on sensitivity to molecular structure have not been thoroughly studied yet. We previously showed that strong field ionization can indeed discern between molecular isomers and stereo isomers in particular.[12]

As part of this project, we have performed experimental studies in this area and have begun corresponding theoretical studies. The experimental work consists of two studies both on the same set of three pairs of molecular isomers C_4H_6, C_4H_8 and C_4H_{10} as shown in Fig. 8. The first study is a wavelength-dependent study of the strong field ionization yields of the three isomers. In this experiment we used femtosecond pulses centered at 800 nm, 1320 nm and 1940 nm. Results of the strong field experiments are shown in Figs. 9 (a) and 9 (b) as a ratio of the parent ion yield between the corresponding isomers as a function of intensity. We should point out that all the measurements were performed on a shot-to-shot basis and corrected by intensity fluctuations and pressure. In addition, all fragments, measured using an ion time of

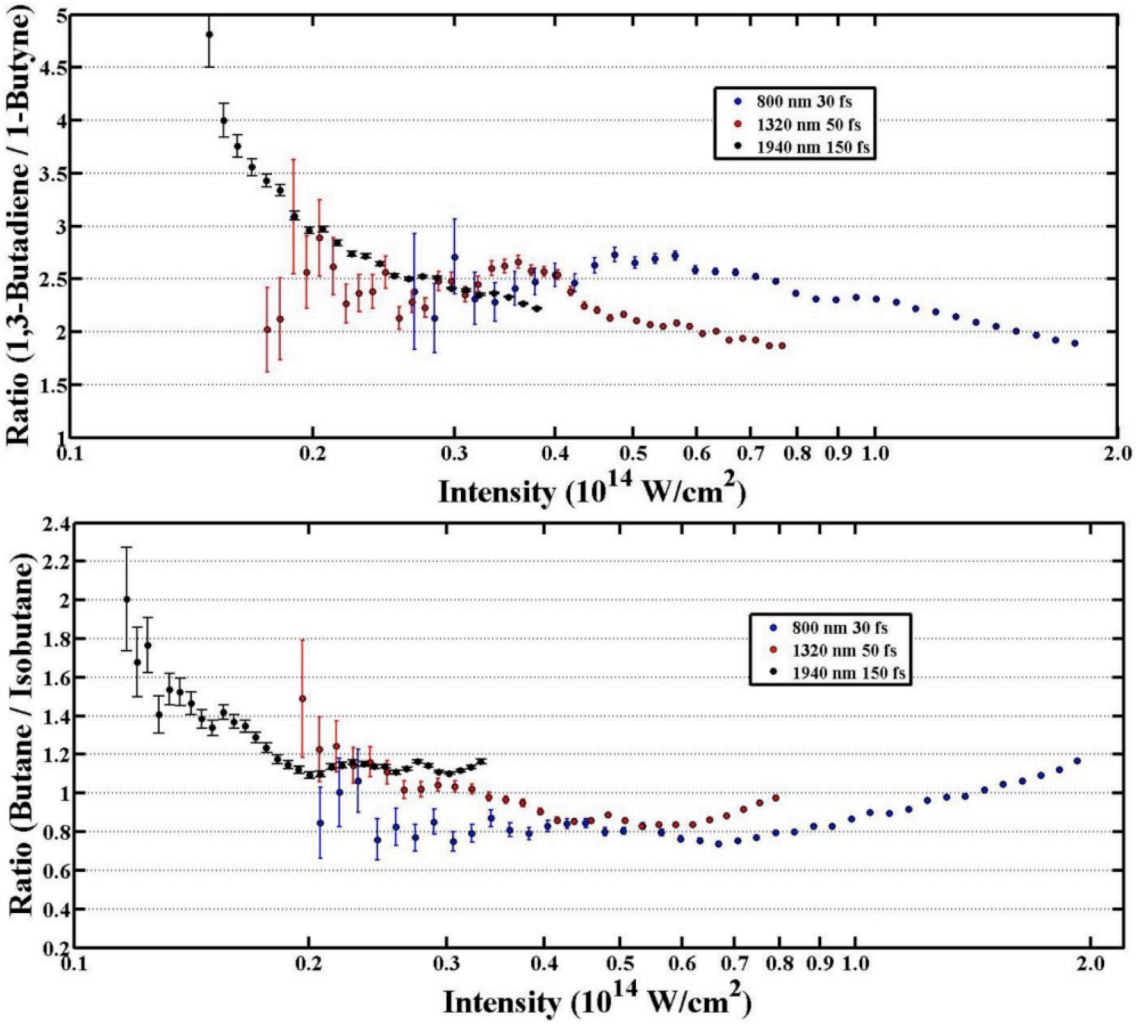

Figure 9. Ratio of the parent ion yield of two molecular isomers as a function of intensity for three different wavelengths. (a) top panel ratio of 1,3 Butadien$^+$ to Butyne$^+$ (b) bottom panel ratio of Butane$^+$ to Isobutane$^+$. Other fragments are also present but omitted for the sake of clarity. Such other fragments become relevant at large intensities, typically around 0.3 – 0.5 $\times 10^{13}$ W/cm^2. Also indicated in the legend is the pulse duration at each of the wavelengths measured using a FROG.

flight (iToF), were also monitored. As expected, at high intensities, fragmentation plays a large role, but we are mainly interested in single ionization events. Thus, the relevant data is at intensities below 5×10^{13} W/cm^2 and a more thorough analysis can be done later to determine the value of intensity at which fragmentation becomes relevant (i.e. > 10% of the parent yield). Since knowledge of the intensity is crucial for these experiments we used a robust fit of the Ar, Kr, and Xe ionization yields to the Yudin-Ivanov ionization model.[13] The atomic yields are measured under the identical conditions as the molecules (focusing, pulse energies, and pulse duration). Pulse durations were measured using a second-harmonic-generation frequency resolved optical gating (FROG) device that was placed within the same optical path of the experimental chamber.

The second set of experiments involved single-photon, weak-field ionization at the advanced light source (ALS). In this set of experiments, the photon energy was the experimental parameter. Ionization dependence with the intensity or fluence has a trivial and known behavior since it is a linear process. As in the case of the strong field experiment, the data was corrected for intensity fluctuations as well as pressure oscillations. The results for the same two pairs of isomers is shown in Fig 10. The photon energy was changed from 20 to 40 eV. All fragments were also monitored but only the parent ions are shown here for clarity since it is the main goal of the study. We should mention however that the fragmentation for these high energy photons is very different than with strong fields.

By comparing the two extreme cases, single vs multiphoton, we see strong differences. Perhaps the most salient difference is that, while the ratio of the yields of the two isomers changes only by up to 15% in the case of weak field ionization, for strong fields the change in ratios can be as large as 400%. The largest change of 400% is measured for the C_4H_6 isomers at 1940 nm. This large ratio is somewhat expected since the difference of I_p (ΔI_p =1eV) is the largest of all isomers. On the other hand, the C_4H_{10} isomers have a very small difference in I_p and yet the ionization yield is very different between the two isomers and shows a marked difference when compared to the ionization of the same isomers by the absorption of a single photon. In addition, the strong field ionization is most differential when using longer wavelengths. This trend can be seen when comparing the ratios at 800 nm vs 1940 nm. This result represents the first of its kind in an attempt to provide a very broad picture of molecular fingerprinting for molecular isomers which represent some of the hardest molecules to identify in chemical and biological systems.

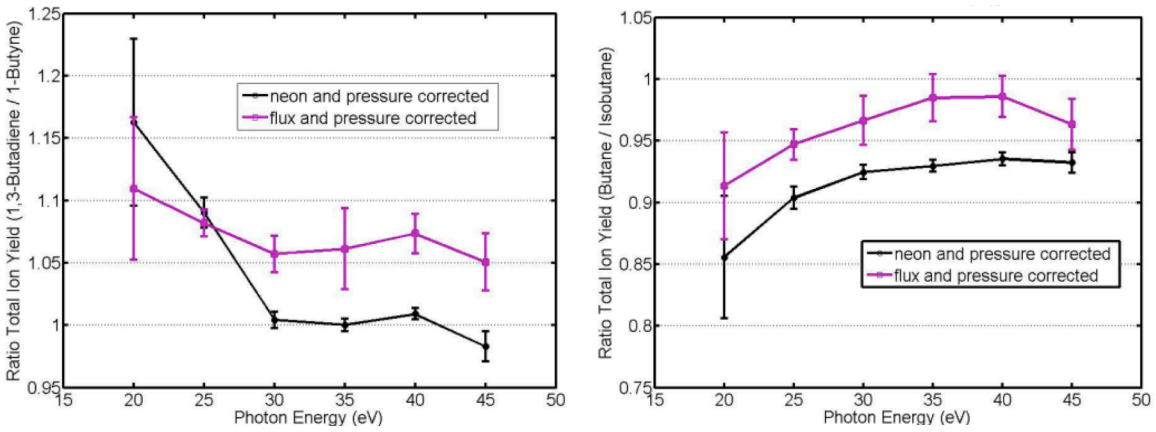

Figure 10. Ratio of the parent ion yield of two molecular isomers as a function of photon energy a) left panel ratio of 1,3 Butadien$^+$ to Butyne$^+$ b) bottom panel ratio of Butane$^+$ to Isobutane$^+$. Other fragments are also present but omitted for the sake of clarity. Intensity of flux correction were performed using two available methods, neon ionization yield or current through a gold mesh.

Experimental Developments

Spatial manipulation of femtosecond pulses for strong field science. We have purchased two spatial light modulators (SLM) for the spatial manipulation of femtosecond pulses. The first SLM has an operating center wavelength of 1100 nm to 1400 nm while the second has an operating center wavelength of 770 nm to 840 nm. In the few months over which this project was active we initiated two main projects.

Attosecond pulse interferometry. We have developed the technique of a self-referencing interferometer by generating harmonics from two sources. Among the measurements that we have been able to perform is the scaling of the harmonics phase with intensity. We have determined that the phase of the high-above-threshold harmonics increases with intensity. On the other hand, the phase of the below-threshold harmonics decreases with intensity. All these measurements were done with 800 nm pulses. We are in the process of improving such phase measurements by using 1400 nm pulses with the SLM purchased through this grant. Using a longer wavelength will allow us to more precisely determine the behavior of the phase with intensity for harmonics near threshold.

Optical parametric amplification beam recycling. One of the most common techniques to generate tunable femtosecond pulses is through the use of an optical parametric amplifier (OPA) which from one 800 nm beam produce a signal and an idler. These devices have typical efficiencies of 30% for the signal and the idler and discard the depleted or remaining of the 800 nm pump beam. We are in the process of using a high-power SLM to demonstrate OPA beam recycling by spatially reshaping the emerging pump beam. Our goal is to be able to reuse the pump beam by enhancing its spatial properties. In this approach an OPA then will generate three usable beams thus increasing the overall efficiency. In particular, we are interested in reusing the 800 nm pump beam for the generation of few-cycle pulses. The experiments uses a close-loop feedback algorithm using the Zernike polynomials as a basis set.

Rescattering Spectroscopy

In collaboration with the group of Kiyoshi Ueda at Tohoku University we have studied rescattering spectroscopy[14] to determine the structure of small hydrocarbons. In particular, we studied the angle-resolved high-energy electron spectra emitted from C_2H_4 in an intense laser field, extracted field-free electron-ion elastic scattering differential cross sections (DCSs) according to quantitative rescattering theory, and obtained molecular contrast factors (MCFs) subtracting the incoherent sum of DCSs of all the atoms in the molecule [12]. Comparing the experimental results of Ueda and coworkers with our computed scattering cross sections and employing least-squares fitting, we have extracted the correct C-C and C-H bond lengths of the molecule within the ~5% uncertainty of the fit. This approach opens the way to retrieve the structure of hydrocarbon molecules, potentially at high temporal resolution, employing low collision energies where electron scattering is sensitive to the hydrogen atoms; and where the independent atom model calculations may fail to reproduce the experimentally extracted MCF.

Coherence in Molecular Photoionization

Another project that is a close collaboration with the AMO theory group at LBNL, is the study of the theory of coherence in ionization of molecules with very short pulses. When a short laser pulse is used to ionize a molecule, and the pulse has a bandwidth that is broad enough to ionize two different ion states with the ejected photoelectron having the same asymptotic kinetic energy from each state, there can be a coherence in the population of the two ionic states.[15] The

coherence comes from photoelectrons emitted from the two ion states that have the same asymptotic momentum, both in magnitude and direction. Thus the coherence will require a non-zero overlap in the molecular frame angle-dependent transition amplitudes. With only an ionization step, the population coherence in the ions, for a system that is not oriented in space, results from an average over all orientations of the molecules with respect to the exciting field and an integration of the product of the emission amplitudes over all photoelectron ejection directions. This can only lead to non-zero coherence when the two ion states have the same symmetry. However, if there is a subsequent probe that takes the system to a common final state, then even with orientation averaging and integration over all photoelectron emission directions, the coherence can be observed more generally. We have developed explicit formulas for computing these coherences that involve the same photoionization amplitudes that are found in expressions for molecular frame photoelectron angular distributions. As illustrative examples, we have applied these theoretical developments to the short pulse ionization of H_2O and glycine ($C_2H_5NO_2$).

Other Photoionization Studies

Photoionization of Linear Alkynes. In our study of the photoionization of a sequence of alkyne molecules [2], we have found a case where channel coupling is very important. In an alkyne molecule there is a C-C triple bond that contains two π bonds. When the molecule has enough symmetry so that these two orbitals are degenerate then a single-channel photoionization calculation done with the full symmetry of the molecule can correctly include the coupling between the two ionization channels using symmetry. When the molecule has lower symmetry, the two π orbitals can have similar energies, but are not degenerate. In such a case it is important to include the two strongly interacting ionization channels in a photoionization calculation, especially to obtain the correct position of shape resonance features.

RFPADS in Non-Linear Molecules Including Molecular Rotation. In a study of the recoil-frame photoelectron angular distributions (RFPADs) of the C $(1s)^{-1}$ photoionization of CH_4 we derived an expression to include the effects of rotation between the time of the photoionization and the subsequent fragmentation of the molecule [5]. We found that computed RFPADs where rotation was included during a 0.5 ps delay between ionization and fragmentation lead to good agreement with the experimental RFPADs for low fragment kinetic energy release (KER). Additionally, the high KER measured RFPADs could be explained using no time delay, suggesting that the different fragment KERs corresponded to different fragmentation pathways with different lifetimes.

Orientation and Alignment of Molecular Ions Produced in Photoionization. In photoionization leading to an excited state of a molecular ion, the polarization of the subsequent fluorescence can yield information about the orientation and alignment of the intermediate ion state.[16] We have derived expressions for this process based on rotation specific photoionization cross sections and then determined the dependence of the fluorescence intensity on the polarization parameters (Stokes parameters) of both incident and emitted light. For the photoionization of N_2 leading to $N_2^+ B\,^2\Sigma_u^+$ state, a comparison of computed fluorescence intensity as a function of its polarization parameters with the experimental results, obtained by J. E. Furst and coworkers at the ALS, shows that the final residual molecular photoion, $N_2^+ X\,^2\Sigma_g^+$, is oriented and this is generally opposite to the direction reached in the simple excitation of the neutral nitrogen molecule by the absorption of circularly-polarized light. This clearly shows that

the ejected electron in the ionization process carries away most of the free angular momentum in the collision.

High Resolution Photoelectron Spectra of Nucleobases. Finally, extensive work was done on single photon photoelectron spectroscopy of nucleobases [1]. Examples of the spectra obtained are shown in Fig. 11. These spectra are the most highly resolved obtained to date, and the increased resolution, and the energy dependent data, provide insights not previously available.

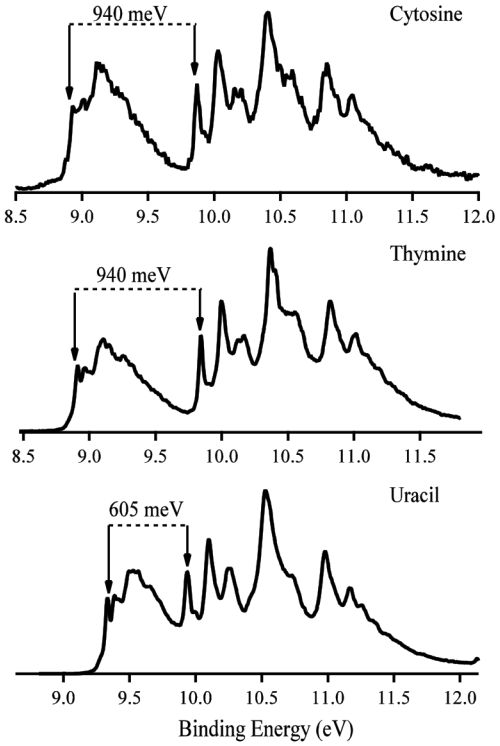

Figure 11. The experimental photoelectron spectra of cytosine (top frame), thymine (middle frame), and uracil (bottom frame) are shown over 3.5 eV energy windows. The intensity scales are arbitrary. Note the energy scales are different for all three spectra. The energy scales have been adjusted to illustrate the strong similarities among all three spectra.

Personnel Training

A significant activity supported by this grant is the training of personnel. During the period of this grant, four graduate students have been supported, Kristen Fulfer (LSU) and Benjamin Wilson (LSU), and Jesus Lopez-Dominguez (TAMU), and Richard Carranza (TAMU). Fulfer, Wilson, and Lopez-Dominguez have successfully completed their Ph.D.'s and have moved on to their next positions. Carranza is still in graduate school. In addition, two postdocs were supported at TAMU, Jobin Jose and Alberto Gonzalez-Castrillo.

References

[1] M. Y. Amusia, N. A. Cherepkov, and L. V. Chernysheva, Phys. Lett. A **40**, 15 (1972).
[2] R. G. Houlgate, J. B. West, K. Codling, and G. V. Marr, J. Electron Spectrosc. Relat. Phenom. **9**, 205 (1976).
[3] A.-T. Le, R. R. Lucchese, S. Tonzani, T. Morishita, and C. D. Lin, Phys. Rev. A **80**, 013401 (2009).
[4] A.-T. Le, R. R. Lucchese, and C. D. Lin, Phys. Rev. A **87**, 063406 (2013).
[5] T. Rescigno and A. Orel, Phys. Rev. A **43**, 1625 (1991).
[6] T. N. Rescigno, B. H. Lengsfield, III, and C. W. McCurdy, in Modern Electronic Structure Theory, edited by D. R. Yarkony (World Scientific, Singapore, 1995), Vol. 1, pp. 501.
[7] F. A. Gianturco, R. R. Lucchese, and N. Sanna, J. Chem. Phys. **100**, 6464 (1994).
[8] L. V. Keldysh, Soviet Physics JETP **20**, 1307 (1965).
[9] D. Pavicic, K. F. Lee, D. M. Rayner, P. B. Corkum, and D. M. Villeneuve, Phys. Rev. Lett. **98**, 243001 (2007).
[10] I. V. Litvinyuk, K. F. Lee, P. W. Dooley, D. M. Rayner, D. M. Villeneuve, and P. B. Corkum, Phys. Rev. Lett. **90**, 233003 (2003).

[11] A. S. Alnaser, S. Voss, X. M. Tong, C. M. Maharjan, P. Ranitovic, B. Ulrich, T. Osipov, B. Shan, Z. Chang, and C. L. Cocke, Phys. Rev. Lett. **93**, 113003 (2004).
[12] S. Zigo, A.-T. Le, P. Timilsina, and C. A. Trallero-Herrero, Sci. Rep. **7**, 42149 (2017).
[13] G. L. Yudin and M. Y. Ivanov, Phys. Rev. A **64**, 013409 (2001).
[14] M. Okunishi, R. R. Lucchese, T. Morishita, and K. Ueda, J. Electron Spectrosc. Relat. Phenom. **195**, 313 (2014).
[15] F. Calegari, D. Ayuso, A. Trabattoni, L. Belshaw, S. De Camillis, S. Anumula, F. Frassetto, L. Poletto, A. Palacios, P. Decleva, J. B. Greenwood, F. Martín, and M. Nisoli, Science **346**, 336 (2014).
[16] E. D. Poliakoff, J. L. Dehmer, D. Dill, A. C. Parr, K. H. Jackson, and R. N. Zare, Phys. Rev. Lett. **46**, 907 (1981).

Products Developed

a) Publications acknowledging DE-SC0012198

Published

1. K. D. Fulfer, D. Hardy, A. A. Aguilar, and E. D. Poliakoff, High resolution photoelectron spectroscopy of the pyrimidine-type nucleobases, *J. Chem. Phys.* **142**, 224310:1-9 (2015). DOI: 10.1063/1.4922310
2. Ugo Jacovella, David Holland, Séverine Boyé-Péronne, Bérenger Gans, Nelson de Oliveira, Kenji Ito, Denis Joyeux, Lucy Archer, Robert Lucchese, Hong Xu, Stephen Pratt, A Near-threshold Shape Resonance in the Valence-shell Photoabsorption of Linear Alkynes, *J. Phys. Chem. A* **119**, 12339-48 (2015). DOI: 10.1021/acs.jpca.5b06949
3. U. Jacovella, D. M. P. Holland, S. Boyé-Péronne, B. Gans, N. de Oliveira, D. Joyeux, L. E. Archer, R. R. Lucchese, H. Xu, and S. T. Pratt, High-resolution vacuum-ultraviolet photoabsorption spectra of 1-butyne and 2-butyne, *J. Chem. Phys.* **143**, 034304:1-14 (2015). DOI: 10.1063/1.4926541
4. J. Jose and R. R. Lucchese, Vibrational effects in the shape resonant photoionization leading to the $A\ ^2T_{1u}$ state of SF_6^+, *Chem. Phys.* **447**, 64-70 (2015). DOI: /10.1016/j.chemphys.2014.12.006
5. Jesús A. López-Domínguez and Robert R. Lucchese, Effects of molecular rotation after ionization and prior to fragmentation on observed recoil-frame photoelectron angular distributions in the dissociative photoionization of non-linear molecules, *Phys. Rev. A* **93**, 033421:1-11 (2016). DOI: 10.1103/PhysRevA.93.033421
6. M. V. Frolov, T. S. Sarantseva, N. L. Manakov, K. D. Fulfer, B. P. Wilson, J. Troß, X. Ren, E. D. Poliakoff, A. A. Silaev, N. V. Vvedenskii, A. F. Starace, and C. A. Trallero-Herrero, "Atomic photoionization experiment by harmonic-generation spectroscopy," *Phys. Rev. A* **93,** 031403(R):1-5 (2016). DOI: 10.1103/PhysRevA.93.031403
7. K. Veyrinas, V. Gruson, S. J. Weber, L. Barreau, T. Ruchon, J. F. Hergott, J. C. Houver, R. R. Lucchese, P. Salieres, and D. Dowek, "Molecular frame photoemission by a comb of elliptical high-order harmonics: a sensitive probe of both photodynamics and harmonic complete polarization state," *Faraday Discuss* **194**, 161-83 (2016). DOI: 10.1039/c6fd00137h
8. B. P. Wilson, K. D. Fulfer, S. Mondal, X. Ren, J. Tross, E. D. Poliakoff, J. Jose, A.-T. Le, R. R. Lucchese, and C. Trallero-Herrero, "High order harmonic generation from SF_6: Deconvolution of macroscopic effects," *J. Chem. Phys.* **145**, 224305 (2016). DOI: 10.1063/1.4971244

9. C.-T. Liao, X. Li, D. J. Haxton, T. N. Rescigno, R. R. Lucchese, C. W. McCurdy, and A. Sandhu, "Probing autoionizing states of molecular oxygen with XUV transient absorption: Electronic-symmetry-dependent line shapes and laser-induced modifications," *Phys. Rev. A* **95**, 043427 (2017). DOI: 10.1103/PhysRevA.95.043427
10. C. W. McCurdy, T. N. Rescigno, C. S. Trevisan, R. R. Lucchese, B. Gaire, A. Menssen, M. S. Schöffler, A. Gatton, J. Neff, P. M. Stammer, J. Rist, S. Eckart, B. Berry, T. Severt, J. Sartor, A. Moradmand, T. Jahnke, A. L. Landers, J. B. Williams, I. Ben-Itzhak, R. Dörner, A. Belkacem, and T. Weber, "Unambiguous observation of F-atom core-hole localization in CF_4 through body-frame photoelectron angular distributions," *Phys. Rev. A* **95**, 011401 (2017). DOI: 10.1103/PhysRevA.95.011401
11. S. M. Poullain, R. Cireasa, C. Cornaggia, M. Simon, T. Marin, R. Guillemin, J. C. Houver, R. R. Lucchese, and D. Dowek, "Spectral dependence of photoemission in multiphoton ionization of NO_2 by femtosecond pulses in the 375-430 nm range," *Phys. Chem. Chem. Phys.* **19**, 21996-2007 (2017). DOI: 10.1039/c7cp02057k

Submitted for publication

12. Yuta Ito, Richard Carranza, Misaki Okunishi, Robert R. Lucchese, and Kiyoshi Ueda, "Extraction of Geometrical Structure of Ethylene Molecules by Laser-Induced Electron Diffraction Combined with Ab Initio Scattering Calculations," *Phys. Rev. A* - submitted for publication.
13. Loren Greenman, Robert R. Lucchese, C. William McCurdy, "Variational treatment of electron-polyatomic molecule scattering calculations using adaptive overset grids," *Phys. Rev. A* - submitted for publication.